Probing Carboxylate Gibbs Transfer Energies via Liquid | Liquid Transfer at Triple Phase Boundary Electrodes: Ion-Transfer Voltammetry versus COSMO-RS Predictions

Stuart M. MacDonald[a], Marcin Opallo[b], Andreas Klamt[c,d], Frank Eckert[c], and Frank Marken[a]*

[a]*Department of Chemistry, University of Bath, Bath, BA2 7AY, United Kingdom*

[b] *Institute of Physical Chemistry, Polish Academy of Sciences, ul. Kasprzaka 44/52, 01-224 Warszawa, Poland*

[c] *COSMOlogic GmbH & Co. KG, Burscheider Str. 515, D-51381 Leverkusen, Germany*

[d] *Institute of Physical and Theoretical Chemistry, University of Regensburg, 93040 Regensburg, Germany*

Corresponding author: Fax: +44 1225 386231 E-mail address: f.marken@bath.ac.uk

Abstract

Understanding liquid | liquid ion transfer processes is important in particular for naturally occurring species such as carboxylates. In this study electrochemically driven mono-, di-, and tri-carboxylate anion transfer at the 4-(3-phenylpropyl)-pyridine | aqueous electrolyte interface is investigated experimentally for a triple phase boundary system at graphite electrodes. The tetraphenylporphyrinato-Mn(III/II) redox system (Mn(III/II)TPP) dissolved in the water-immiscible organic phase (4-(3-phenylpropyl)pyridine) is employed for the quantitative study of the structure – Gibbs transfer energy correlation and the effects of the solution pH on the carboxylate transfer process. For di- and tri-carboxylates the partially protonated anions are always transferred preferentially even at a pH higher than the corresponding pK_A. COSMO-RS computer simulations are shown to provide a quantitative rationalisation as well as a powerful tool for predicting Gibbs free energy of transfer data for more complex functionalised carboxylate anions. It is shown that the presence of water in the organic phase has a major effect on the calculated Gibbs free energies.

1. Introduction

Processes at liquid | liquid interfaces [1] are ubiquitous and important both in nature (e.g. in membrane processes, proton pumps, drug transport, etc.) and in technology (e.g. in phase transfer reactions, extraction processes, sensors, etc.). Interest in the electrochemistry of these types of processes dates back to early ion transfer studies by Nernst and coworkers [2,3]. More recently, a range of novel methodologies have been developed based on the direct polarisation of liquid | liquid interfaces with two adjacent electrolyte supported immiscible liquids [4,5,6]. Large surface area studies [7] as well as microhole [8] or even nanohole [9,10] experiments, the use of membrane-modified liquid | liquid interfaces [11,12], or hydrodynamic measurements [13] are possible. By reducing the size of the organic phase to microdroplet dimensions, the experiment can be further simplified and the need for supporting electrolyte in the organic phase avoided [14]. The microdroplet phase forms a triple phase boundary [15] which allows ion transfer processes to be studied for anions [16] as well as for cations [17]. Over the recent years several studies addressed the need for inert redox systems [18], the quantitative data analysis [19], new mechanistic insights [20], novel electrode designs based on array surface patterning [21], wire-intersected liquid|liquid interfaces [22], or mesoporous films to host the organic microdroplet phase [23,24], and microfluidic methodologies [25] for monitoring triple phase boundary processes.

A range of standard anions, such as PF_6^-, ClO_4^-, SCN^-, NO_3^-, Cl^-, F^- etc. is commonly employed in electrochemical ion transfer studies [26]. These anions offer a useful diagnostic range of Gibbs free energy of transfer characteristics. They exhibit an approximately spherical charge distribution which is important for the approximate correlation of data for example to the inverse ion radii employing the Born model [27]. Scholz et al. [28] have considerably widened the applicability of the triple phase boundary based electrochemical method by investigating the transfer of amino acids, peptides, and small proteins [29,30]. The transfer of carboxylate mono-anions was investigated for the water | nitrobenzene interface employing the decamethylferrocene$^{+/0}$ redox system [31]. The transfer of ionic drugs in biological water | lipid interfacial systems and cell membranes is a closely related phenomenon

where Gibbs free energy of transfer information is essential.

There has been no comparative study into the liquid | liquid transfer properties of mono-, di-, and tri-carboxylates and in this study a first quantitative comparison is attempted taking into account the effect of pH. First, it is established that well behaved liquid | liquid anion transfer is observed when the organic solvent soluble $Mn(III/II)TPP^{+/0}$ redox system is employed in a 4-(3-phenylpropyl)-pyridine (PPP) solvent. This solvent aides MnTPP solubility and PPP coordination at the Mn(III/II) metal center is believed to suppress binding of other nucleophiles. Microdroplet deposits on a basal plane pyrolytic graphite electrode surface are employed and the $Mn(III/II)TPP^{+/0}$ redox process is shown to lead (in most cases) to simple anion transfer (see Figure 1). The formation of $Mn(III)TPP^+$ is indicated as a positive charge (plus symbol) which is resulting in the transfer of an anion, X^-, from the aqueous into the organic droplet phase in order to maintain charge neutrality in the organic phase [32]. In this study, different types of anions are compared and the dramatic effect of pH on the transfer process is established. Finally, COSMO-RS calculations are employed to explain quantitative trends in the data on a molecular level. The agreement of electrochemical experiment and the COSMO-RS results is shown to be excellent when the presence of water partitioned into the organic phase is taken into consideration. COSMO-RS is a powerful tool for (i) the prediction of transfer potentials or ionic Gibbs transfer energies and (ii) protonation effects for more complex and highly functionalised molecular structures. In future, COSMO-RS calculations could be used to also "map" the energy profile for the transition of an ion across the liquid | liquid phase boundary.
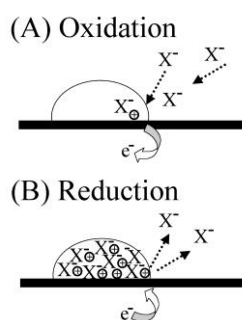

Figure 1. Schematic drawing of the anion transfer at immobilised microdroplets at electrode surfaces during oxidation (uptake of anions from the aqueous into the organic phase) and reduction (expulsion of anions from the organic into the aqueous phase).

2. Experimental

2.1. Reagents

Sodium perchlorate (99%, Aldrich), KCl (analytical grade, Aldrich), sodium acetate (99%, Aldrich), acetic acid (>99.7%, Aldrich), sodium chloroacetate (99%, Aldrich), sodium trichloroacetate (99%, Aldrich), sodium nitrate (99%, Aldrich), potassium hexafluorophosphate (99%, Aldrich), sodium malonate (99%, Aldrich), malonic acid (99%, Aldrich), sodium citrate (99%, Aldrich), citric acid (99%, Aldrich), sodium succinate (99%, Aldrich), succinic acid (99%, Aldrich), sodium fumarate (98%, Aldrich), fumaric acid (99%, Aldrich), sodium maleate (Fluka, 98%), maleic acid (99%, Aldrich), 5,10,15,20-tetraphenyl-21H,23H-porphine manganese(III) chloride (95%, Aldrich), 4-(3-phenylpropyl)-pyridine (PPP) (97%, Aldrich), and acetonitrile (HPLC grade, Aldrich) were all purchased in analytical grade and used without further purification. Filtered and demineralised water was taken from an Elga water purification system with not less than 18 MOhm cm resistivity. Buffer solutions were prepared for each pH by dissolving appropriate amounts of carboxylate and carboxylic acid.

2.2. Instrumentation

Voltammetric measurements were conducted with a μ-Autolab III potentiostat system (Eco Chemie, The Netherlands) in a conventional three-electrode electrochemical cell. Experiments were performed in staircase voltammetry (typically 1 mV step potential) mode with a platinum gauze counter electrode and a saturated calomel reference electrode (SCE, REF401, Radiometer). The working electrode was a 4.9 mm diameter basal plane pyrolytic graphite electrode (Pyrocarbon, Le Carbone, UK). The graphite electrode was cleaned by polishing on a fine carborundum paper (Buehler, P1200) prior to each use. All pH measurements were conducted using a Fisherbrand Hydrus 300 system. The water content of 4-(3-phenylpropyl)-pyridine was determined as 55 mol% (or ca. 5 wt%) after two-phase equilibration of 4-(3-phenylpropyl)pyridine (PPP) with aqueous 0.1 M $NaClO_4$ and recording ^{1}H-nmr in CD_3CN (Bruker 300 MHz ICON NMR). Aqueous solutions were thoroughly de-aerated with argon (BOC) prior to conducting experiments. Experiments were conducted at a temperature of 22 ± 2°C.

2.3. Procedures

The deposition solution was prepared by initially dissolving 4 mg 5,10,15,20-tetraphenyl-21H,23H-porphine manganese (III) chloride (MnTPPCl) in 80 mg 4-(3-phenylpropyl)-pyridine (PPP) (with gentle heating). Acetonitrile (10 cm^3) was then added to the resulting dark green viscous oil and the resulting dark green solution sonicated to give a homogeneous solution. A fresh deposition solution in acetonitrile was prepared daily. An optimum volume (10 µL, vide infra) of the resulting deposition solution was placed onto the 4.9 mm diameter basal plane pyrolytic graphite electrode surface. Subsequent evaporation of the acetonitrile phase left an electrochemically active PPP microdroplet deposit on the electrode surface [33]. The electrode was then immersed into aqueous electrolyte solution for voltammetric experiments. After use, the electrode was renewed by polishing on carborundum paper.

2.4. COSMO-RS Calculations

COSMO-RS, i.e. the conductor-like screening model for realistic solvation [34,35,36], is a relatively novel method to predict thermodynamic properties of neutral and charged molecules in liquids. It starts from the polarization charge densities of the solute and solvent molecules in a virtual conductor embedding the molecules. These can be efficiently calculated in density function theory (DFT) quantum chemical calculations employing the conductor-like screening model (COSMO) [37] which is nowadays available in most quantum chemical programs. The TURBOMOLE program [38] with a Becke-Perdew functional [39,40] and a TZVP basis set was used for these calculations, together with the default COSMO parameters in TURBOMOLE.

In a second step, the COSMO-RS method expresses the specific interactions of molecules in a liquid system, i.e. electrostatic interactions and hydrogen bonding, as local pair-wise interactions of surface interactions quantified by the COSMO polarization charges densities σ and σ' of the interacting surfaces. Finally an efficient

and accurate statistical thermodynamics calculation is performed for the interacting surfaces, yielding the chemical potentials and free energies of the molecules in pure and mixed solvents, at variable temperature. Meanwhile COSMO-RS has been widely validated in physical chemistry and chemical engineering applications with respect to all kinds of equilibrium properties, as partition and activity coefficients, vapour pressures, solubilities, pK_a-values, for ionic liquids, and even for polymers and bio-membranes. It should be noted that COSMO-RS is exclusively developed and parameterized on data of neutral compounds. Its success for ions purely results form its inherent predictive power for extrapolation to new systems. Standard COSMO-RS calculations have been performed with the COSMOtherm program with the BP_TZVP_C21_0107 parameterization [41]. Multiple conformations have been taken into account for the ions in a self-consistent way. This is of special importance for the multiple carbonic acids, which can form complex intramolecular hydrogen bond patterns in the neutral form and even more in partially deprotonated ions.

3. Results and Discussion

3.1. Electrochemically Driven Carboxylate Transfer Processes at Aqueous Electrolyte | 4-(3-Phenylpropyl)-Pyridine Interfaces

Initially, the transfer of simple anions and that of carboxylates are compared. The measurement is based on the deposition of a random array of microdroplets of 4-(3-phenylpropyl)-pyridine (or PPP), a water immiscible organic oil, onto a basal plane pyrolytic graphite electrode surface [27]. Dissolved into the PPP phase is a reversible one electron redox system, tetraphenylporphyrinato-Mn(III) chloride (or MnTPPCl). Figure 2A shows typical cyclic voltammograms obtained for the reduction and re-oxidation of $MnTPP^+$ (70 mM MnTPPCl in PPP; the Cl^- is rapidly exchanged and not observed; $MnTPP^+$ is believed to form a solvate complex with the PPP solvent) immersed in aqueous 0.1 M $NaClO_4$ as a function of the deposition volume. The reduction and re-oxidation of $MnTPP^+$ is coupled to the transfer of anions between the organic and the aqueous solution phase [27]. The volume (or coverage) of PPP oil deposit is an important parameter. Increasing the volume of oil deposit is initially

increasing the voltammetric response (more MnTPP is immobilised at the electrode surface) but then the voltammetric response (which originates from the triple phase boundary) is decreasing due to partial blocking of the basal plane pyrolytic graphite electrode surface with the non-conducting PPP oil phase. An optimum is reached with a 10 µL deposit for a 4.9 mm diameter electrode surface (resulting in ca. 80 nL PPP microdroplets distributed over the surface) and this deposition volume is then used throughout this study.
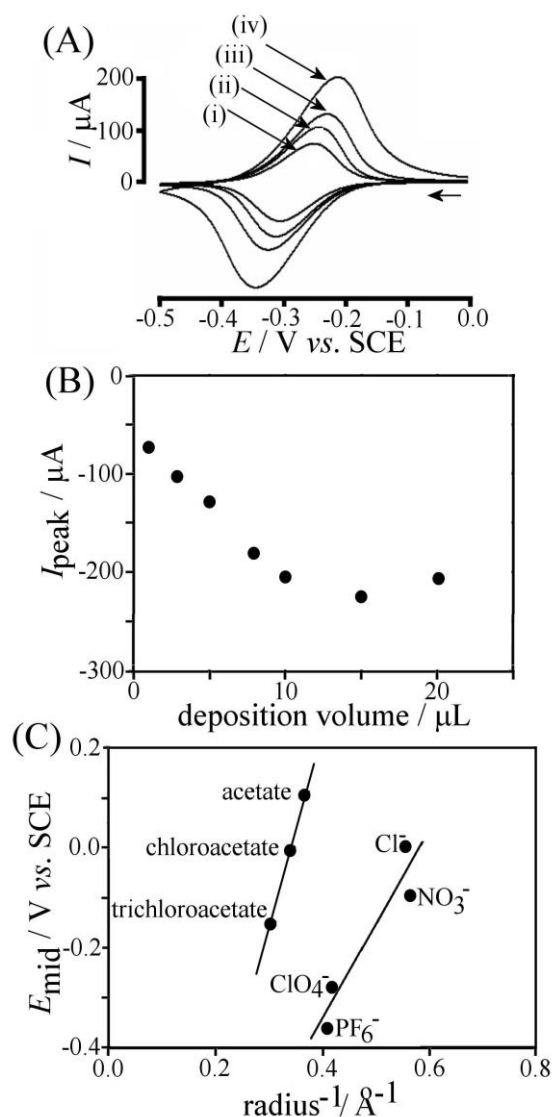

Figure 2. (A) Cyclic voltamograms (scan rate 50 mV s^{-1}) for the reduction and re-oxidation of 70 mM MnTPP$^+$ in PPP (see Experimental) deposited onto a 4.9mm diameter basal pyrolytic graphite electrode. The modified electrode is immersed in a de-aerated aqueous 0.1 M NaClO$_4$. Deposition volume (i) 1 µL, (ii) 3 µL, (iii) 5 µL, and (iv) 10 µL. (B) Plot of the cathodic peak current versus the deposition volume of the acetonitrile solution. (C) Plot of the midpoint potentials (obtained in aqueous 0.1 M electrolyte media) versus the inverse radius (approximate) for a range of different anions employed in this study.

The voltammetric responses in Figure 2A shows well defined anodic and cathodic peak features and the analysis of these data is possible in terms of the midpoint potential, E_{mid} [27], which is determined as the midpoint between oxidation and reduction peak potential (equation 1).

$$E_{mid} = \frac{E_p^{ox} - E_p^{red}}{2}$$ (1)

When immersed in other types of electrolyte solution, the anion transfer process at the modified electrode is observed at a characteristically shifted midpoint potential [27]. The analysis of the midpoint potential data for different types of anions can therefore be employed to characterise the transfer characteristics or to determine the Gibbs energy of transfer for a range of anions. A very approximate approach, useful in particular for spherical anions [27] is the Born plot (here a plot of the midpoint potential versus the inverse of the approximate radius, see Figure 2C). The plot demonstrates a dramatic difference in behaviour when comparing the almost spherical anions (PF_6^-, ClO_4^-, NO_3^-, Cl^-) with a range of typical carboxylates (acetate, monochloroacetate, trichloroacetate). There is no common trend due to the highly non-symmetric charge density distribution in carboxylate anions. Any general correlation attempt of midpoint potential data for carboxylate anions will therefore be strongly dependent on taking into account the geometry and local anion-solvent interactions (vide infra). Next, in order to more quantitatively validate the thermodynamic significance of the midpoint potential data, the effect of anion and redox system concentrations on the voltammetric response are investigated.
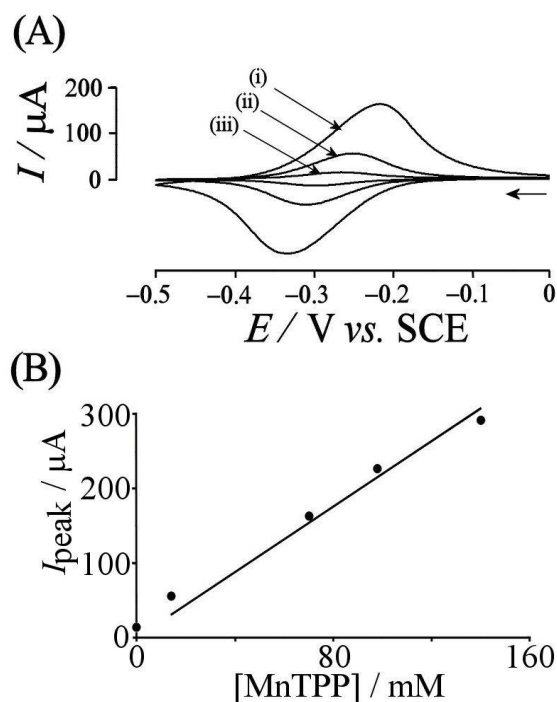
9

Figure 3. (A) Cyclic voltamograms (scan rate 50 mVs⁻¹) for the reduction and re-oxidation of (i) 70 mM (ii) 14 mM and (iii) 0.25 mM MnTPP⁺ in PPP deposited onto a 4.9 mm diameter basal pyrolytic graphite electrode. In each case the modified electrode is immersed into a de-aerated aqueous solution of 0.1 M NaClO₄. (B) A plot of anodic peak current for the oxidation of MnTPP(II) to MnTPP(III) versus the concentration of MnTPP⁺ deposited onto the working electrode.

The concentration of MnTPP⁺ in the organic phase can be seen to directly affect the peak current of voltammograms (see Figure 3) with an approximately linear correlation. Interestingly, the midpoint potential of the voltammetric response is virtually independent of the MnTPP⁺ concentration over the concentration range studied. In contrast, the aqueous electrolyte solution concentration clearly does affect the midpoint potential (see Figure 4A) and the dependency is in good approximation Nernstian (ca. 58 mV shift in midpoint potential for each decade change in concentration). Only at higher concentration activity coefficient effects become significant.

The midpoint potential data has been proposed to be linked to the Gibbs energy of transfer (for anions transferring across the liquid | liquid phase boundary) by the appropriate Nernst equation [42] (see equation 2; written in terms of concentrations

and therefore ignoring the effects of activity coefficients; this expression is also ignoring the effect of placing the reference electrode into the aqueous phase rather than into the organic phase where the redox process occurs).

$$E = E_{Ox_{org}/\mathrm{Re}\,d_{org}}{}^{\theta} + \Delta\phi_{aq}{}^{org}{}_{A^-}{}^{\theta} + \frac{RT}{F}\ln\left(\frac{[Ox_{org}][A_{org}{}^-]}{[\mathrm{Re}\,d_{org}][A_{aq}{}^-]}\right) \tag{2}$$

In this equation for a one electron process, the potential E is determined by the standard redox potential $E_{Ox_{org}/\mathrm{Re}\,d_{org}}{}^{\theta}$, the standard transfer potential for the anion A^-, $\Delta\phi_{aq}{}^{org}{}_{A^-}{}^{\theta}$, and the concentrations of Ox, Red, and the transferring anion in organic and aqueous phase. For the conditions which apply at the potential half way between oxidation and reduction response a modified equation (see equation 3) has been proposed [42]. In this equation the initial concentration of the redox system is set to $[Ox_{org}] = [\mathrm{Re}\,d_{org}] = \frac{c_0}{2}$ (with c_0 denoting $[Ox_{org}] + [Red_{org}]$) and the concentration of anions in the organic phase is $[A_{org}{}^-] = \frac{c_0}{2}$.

$$E_{mid} \approx E_{Ox_{org}/\mathrm{Re}\,d_{org}}{}^{\theta} + \Delta\phi_{aq}{}^{org}{}_{A^-}{}^{\theta} + \frac{RT}{F}\ln\left(\frac{c_0}{2}\right) - \frac{RT}{F}\ln[A_{aq}{}^-] \tag{3}$$

Experimentally, it can be shown that the term $\frac{RT}{F}\ln\left(\frac{c_0}{2}\right)$ remains insignificant (vide supra, possibly due to ion association or kinetic effects) and a simplified empirical expression for the transfer of an anion A^{n-}, can be derived (see equation 4).

$$E_{mid} \approx E_{ref} + \Delta\phi_{aq}{}^{org}A^{n-\theta} - \frac{RT}{nF}\ln[A_{aq}{}^{n-}] \tag{4}$$

An estimate for $\Delta\phi_{aq}^{\;org}A^{n-\theta}$ is therefore obtained from midpoint potential data extrapolated to the point of unit electrolyte concentration (or activity) and taking into account the appropriate reference scale given by the E_{ref} value [43]. The Gibbs transfer energy $\Delta G_{aq}^{\;org}{}_{A^-}^{\;\theta} = nF\,\Delta\phi_{aq}^{\;org}{}_{A^-}^{\;\theta}$ is dominated by the solvation energies in the aqueous and (to a lesser extent) in the organic phase. This difference in solvation energies, even for complex multi-functional anions or uncommon solvents, can be predicted by the COSMO-RS approach. Therefore, this study is aiming at correlating the estimate of the Gibbs transfer energies obtained from electrochemical data to data based on the COSMO-RS prediction (see Experimental).

3.2. Anion Concentration Effects on Liquid | Liquid Carboxylate Transfer Processes

In order to assess the validity of the assumption of anion transfer, the Nernstian slope with respect to the aqueous anion concentration can be investigated. The anion transfer process, in particular for multiply charged anions, could be affected by simultaneous cation transfer (as demonstrated for example for the case of phosphate transfer [44]) and the description in terms of the appropriate Nernst equation (see equation 3) therefore needs to be verified experimentally for each anion.
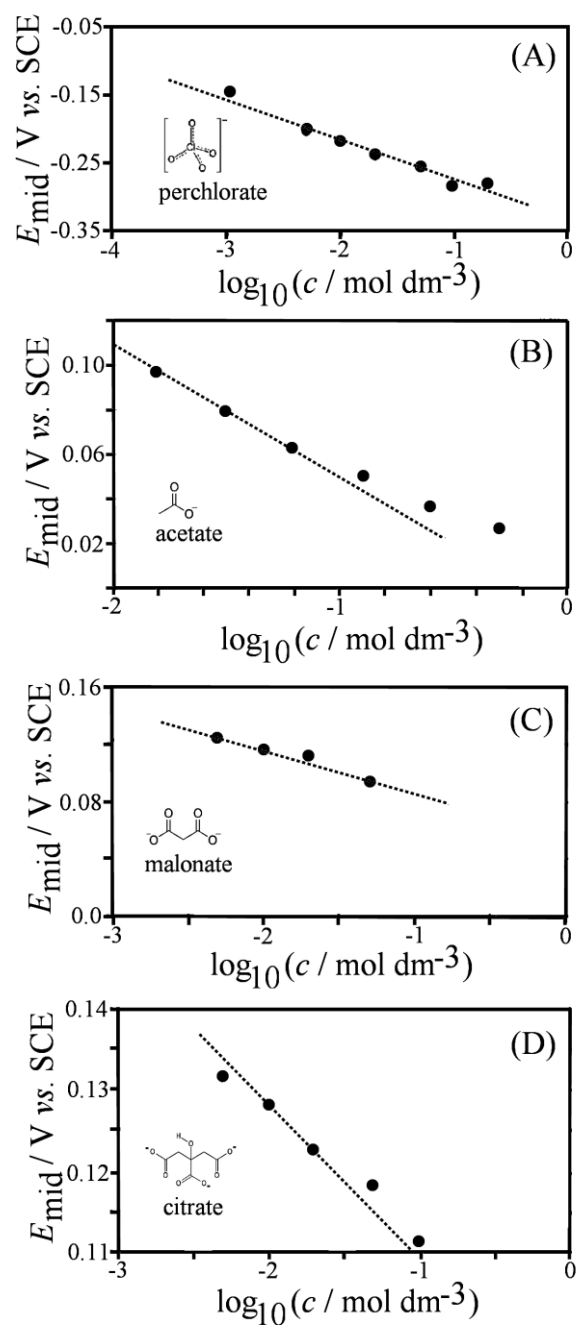
Figure 4. Voltammetric data (scan rate 50 mV s^{-1}) for the transfer of anions as a function of aqueous electrolyte concentration. (A) Plot of E_{mid} versus NaClO$_4$ concentration with a dotted line indicating the predicted slope of -0.058 V per decade change in concentration. (B) Plot of E_{mid} versus Na$^+$ acetate concentration with a dotted line indicating the predicted slope of -0.058 V per decade change in concentration. (C) Plot of E_{mid} versus Na$^+$ malonate concentration with a dotted line indicating the predicted slope of -0.028 V per decade change in concentration. (D) Plot of E_{mid} versus Na$^+$ citrate concentration with a dotted line indicating the predicted slope of -0.019 V per decade change in concentration.

Figure 4A shows a typical plot for data obtained for the perchlorate transfer over a range of aqueous $NaClO_4$ concentrations (1 mM to 200 mM). As the concentration of the perchorate in the aqueous phase is reduced the midpoint potential is shifted more positive as expected. The shift in potential is approximately 58 mV per decade change in concentration (ignoring the effect of activity coefficients) and this is in excellent agreement with equation 4 assuming the transfer of a mono-anion.

The analysis of the midpoint potential for the transfer of acetate anions is shown in Figure 4B. Again a trend and slope consistent with the transfer of a mono-anion is observed. More interesting is the case of di-carboxylates such as malonate. The di-anions show voltammetric features very similar to those for the mono-anions and the transfer process occurs in a similar potential range. However, the slope of the plot of E_{mid} versus logarithm of concentration (see Figure 4C) clearly shows a different trend and is consistent with the Nernst equation for di-anion transfer (slope 28 mV per decade change in concentration, equation 4). Very similar results were obtained with fumarate, maleate, and succinate confirming the 2-electron transfer per di-anion transferred in these cases. Finally, the case of a tri-anion is investigated. Citrate (see Figure 4D) has been chosen as the model case and the slope of the E_{mid} versus logarithm of concentration plot again is consistent with a multi-electron case in reasonable agreement with the appropriate Nernst expression (slope 19 mV per decade change in concentration, equation 4). These data confirm that the transfer of mono- or multiply charged carboxylates can be understood as a simple process in which the charge due to electron transfer within the organic phase is balanced by the appropriate amount of anions from the water into the organic phase.

Next, the effect of the proton activity (or concentration) within the aqueous phase is considered as the key parameter in changing the charge state (and therefore the transfer characteristics) of the carboxylate anions.

3.3. Proton Concentration Effects on Liquid | Liquid Carboxylate Transfer Processes

The concentration of carboxylate anions is dependent on the proton activity in solution and therefore experiments conducted as a function of pH allow anion transfer processes to be studied and understood in more detail. Initially, the transfer of acetate anions is investigated over a pH range of 2 to 8 (see Figure 5A). At sufficiently alkaline pH no significant change in the voltammetric responses occurs and the midpoint potential remains stable since all acetate ions remain in the deprotonated state. At a pH close to the $pK_{A1} = 4.75$ of acetate [45], the voltammetric signal then starts to shift positive which is consistent with a lowering of the concentration of acetate anions in the aqueous solution phase. The acetate transfer is becoming more difficult due to protonation.

In contrast, the behaviour observed for the transfer of di- or tri-anions is very different. The plot in Figure 5B demonstrates that the midpoint potential in the case of succinate transfer is shifting to more *negative* potentials at lower pH in contrast to the behaviour observed for acetate. This effect can be rationalised when considering the Gibbs energy of transfer for the semi-protonated succinate mono-anion. This mono-anion will be considerably more hydrophobic and therefore associated with a different (more favourable) Gibbs energy of transfer. An estimate for this value can be obtained from the region of constant E_{mid} at about pH 4 (see dotted line). A summary of estimated Gibbs free energy of transfer data from electrochemical experiments for a range of anions is given in Table 1.
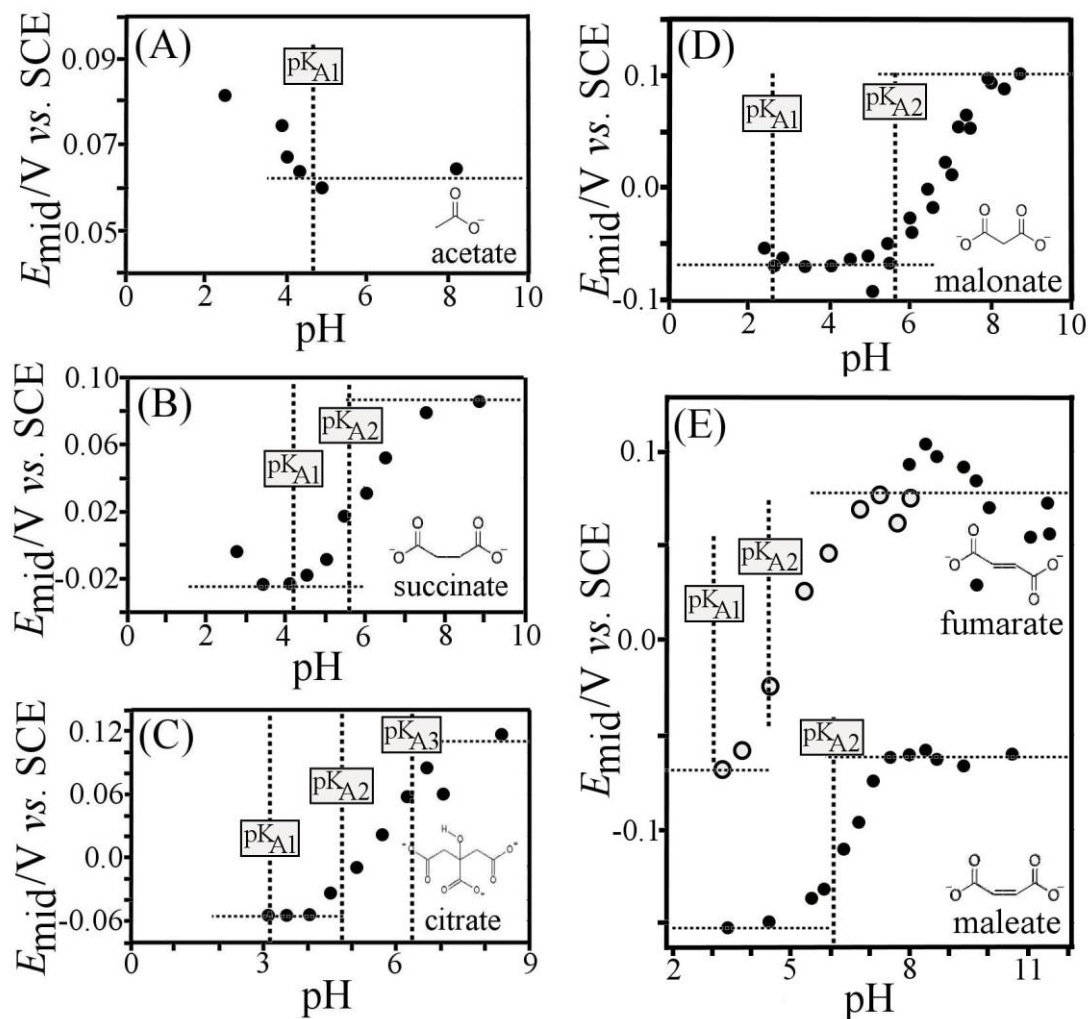
Figure 5. Plots for the midpoint potential (determined with a 70 mM MnTPP$^+$ solution in PPP immersed in 0.1 M aqueous electrolyte) versus the pH for (A) acetate, (B) succinate, (C), citrate, (D) malonate, (E) fumarate and maleate. The dashed lines indicate literature values for the pK$_A$ [45].

Consistently, the shift in E_{mid} potential for succinate as well as for all other di- and tri-anionic carboxylates occurs 2-3 pH units prior to the pK$_A$ values where a significant shift is expected (see Figure 5B-E). This behaviour is not surprising as the protonated form of the anion is the energetically preferred form in the organic phase and the transfer of the protonated form is effective already at a very low concentration. A more quantitative analysis of this effect at low buffer capacity is complicated by the possibility of localised pH gradients at the liquid | liquid interface under potentiodynamic conditions.
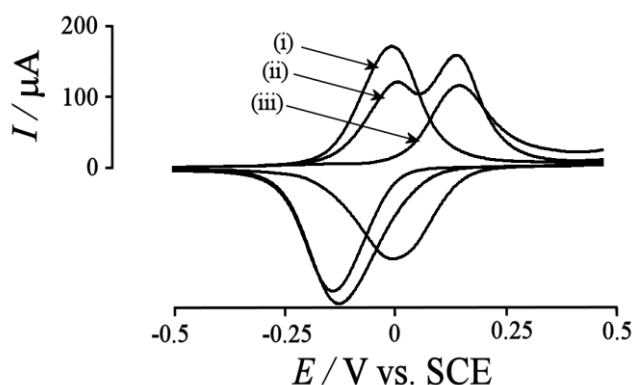
Figure 6. Cyclic voltamograms (scan rate 50 mVs⁻¹) for the reduction and re-oxidation of 70 mM MnTPP⁺ deposited onto a 4.9 mm diameter basal plane pyrolytic graphite electrode and immersed in a 0.1 M solution of sodium maleate (at (i) pH 7.11, (ii) pH 8.41, and (iii) pH 10.05).
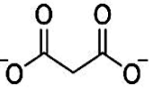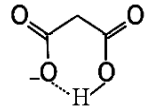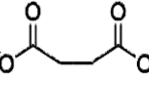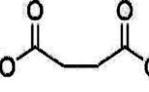
Perhaps surprisingly, the transfer of maleate di-anions was observed to be more complex than expected for a simple liquid | liquid anion transfer (see Figure 5E). An interesting effect is observed for the transfer of maleate across the liquid | liquid boundary over the pH range 7.5 to 10. At pH 7.11 the cyclic voltammogram (see Figure 6i) appears simple (however, with a midpoint potential inconsistent with dianion transfer, vide infra). At pH 8.41 (see Figure 6ii) a second more positive anodic peak is dominant, whereas the initial oxidation peak has significantly diminished in magnitude. Once the pH has been raised to 10.05 (see Figure 6iii), the initial signal has disappeared completely to be replaced by the peak at more positive potential. The transfer of maleate dianions is expected to occur at a potential very close to that for fumarate dianions and therefore at sufficiently alkaline pH dianion transfer appears to be the mechanism. However, when the proton activity is increased a new process is beginning to occur for maleate and it seems plausible that the chelating cyclic structure of the protonated maleate mono-anion is causing a very effective transfer into the organic phase. Interaction of the maleate dianion with the MnTPP(III) cation could then result in the unusual characteristics observed in these experiments. The transferring ionic species for the intermediate pH range (pH 7- pH 10) remains unclear and only in the more acidic pH range transfer of the protonated
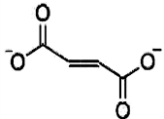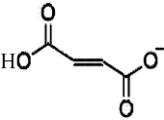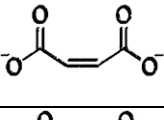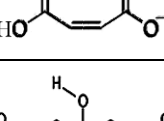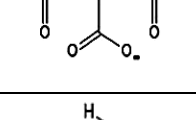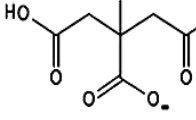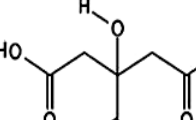
maleate monoanion is proposed. These conclusions are in agreement with the analysis of the correlation of electrochemical data with predictive COSMO-RS data (vide infra).

3.4. COSMO-RS Calculation of Gibbs Free Energy of Transfer Effects for Liquid | Liquid Carboxylate Transfer Processes

The quantitative understanding and prediction of liquid | liquid ion transfer processes for more complex anion structures is important in particular for non-spherical and multi-functional anions. Here the experimental data are compared with COSMO-RS calculations predicting the Gibbs free energy of transfer. Calculations have been performed by transferring the anions from water into 4-(3-phenyl-propyl)-pyridine (PPP). Data in Table 1 summarise the experimental midpoint potential data (extrapolated to unit activity and placed on an appropriate reference scale, see equation 4), the corresponding experimental Gibbs free energy of transfer data, and COSMO-RS results for the Gibbs free energy of transfer for three different organic solvent environments: (i) dry nitrobenzene, (ii) dry PPP, and (iii) wet PPP (containing 55 mol% water).

Table 1. Summary of anion transfer data obtained from voltammetric measurements and from COSMOtherm calculation (see Experimental). Experimental midpoint potential data were obtained at 0.1 M aqueous electrolyte concentration and extrapolated to 1.0 M activity.

Anion system	Structure	Charge state	E_{mid}(0.1 M) / V vs. SCE (a)	E_{mid}(1 M) / V vs. SCE (b)	E_{mid}(1 M) - E_{ref} / V vs. SCE (c)	$\Delta G_{aq}^{org}(A^{n-})_{EC}^{\ominus}$ / kJmol^{-1} (d)	$\Delta G_{aq}^{org}(A^{n-})_{COSMO\text{-}RS}^{\ominus}$ / kJmol^{-1} (e)	$\Delta G_{aq}^{org}(A^{n-})_{COSMO\text{-}RS}^{\ominus}$ / kJmol^{-1} (f)	$\Delta G_{aq}^{org}(A^{n-})_{COSMO\text{-}RS}^{\ominus}$ / kJmol^{-1} (g)
chloride	Cl^-	-1	0.002	-0.057	0.363	35	106.4	115.7	63.4
nitrate	NO_3^-	-1	-0.097	-0.156	0.264	25	68.3	75.3	54.7
perchlorate	ClO_4^-	-1	-0.276	-0.335	0.085	8.2	34.1	39.2	34.1
hexafluoro-phosphate	PF_6^-	-1	-0.361	-0.420	0 (c)	0 (d)	9.10	15.6	13.9
acetate	CH_3COO^-	-1	0.058	-0.001	0.419	40	103.7	112.6	50.3
monochloro-acetate	$ClCH_2COO^-$	-1	-0.007	-0.066	0.354	34	81.4	89.3	47.2
trichloro-acetate	Cl_3CCOO^-	-1	-0.162	-0.221	0.199	19	48.0	53.5	33.2
malonate		-2	0.102	0.072	0.492	95	221.9	239.9	109.2
		-1	-0.068	-0.127	0.293	28	68.7	75.9	51.2
succinate		-2	0.083	0.053	0.473	91	209.7	226.7	103.1
		-1	-0.023	-0.082	0.338	33	71.6	79.2	51.4

fumarate		-2	0.076	0.046	0.466	90	195.6	212.1	102.8
		-1	-0.069	-0.128	0.292	28	90.5	84.5	46.8
maleate		-2	-0.061 (h)	-0.091	0.329	63	210.2	228.0	108.9
		-1	-0.153	-0.212	0.208	20	61.1	67.9	45.8
citrate		-3	0.115	0.095	0.515	149	349.9	377.8	167.2
		-2		-0.060	0.360	69	151.8	165.9	108.5
		-1	-0.054	-0.113	0.307	30	42.9	42.0	35.0

(a) taken from data in Figure 4 and 5.

(b) extrapolated by assuming Nernstian shifts (58 mV for A^-, 28 mV for A^{2-}, and 19 mV for A^{3-})

(c) the reference point for a SCE reference electrode is approximately achieved at the point of transfer for the PF_6^- anion (E_{ref} = -0.420 V). The resulting scale is consistent with literature data [43].

(d) calculated from $\Delta G_{aq}^{org}{}_{A^-}^{\theta} = nF\, \Delta\phi_{aq}^{org}{}_{A^-}^{\theta}$ and $\Delta\phi_{aq}^{org}{}_{A^-}^{\theta} = E_{mid}(1M) - E_{ref}$

(e) calculated with COSMOtherm for dry nitrobenzene, see Experimental

(f) calculated with COSMOtherm for dry 4-(3-phenylpropyl)pyridine, see Experimental

(g) calculated with COSMOtherm for wet 4-(3-phenylpropyl)pyridine with 55 mol% water, see Experimental

(h) the correct value for the maleate dianion is experimentally essentially identical to that of the fumarate dianion and therefore the second more negative voltammetric response (unknown mechanism) is included at this point.
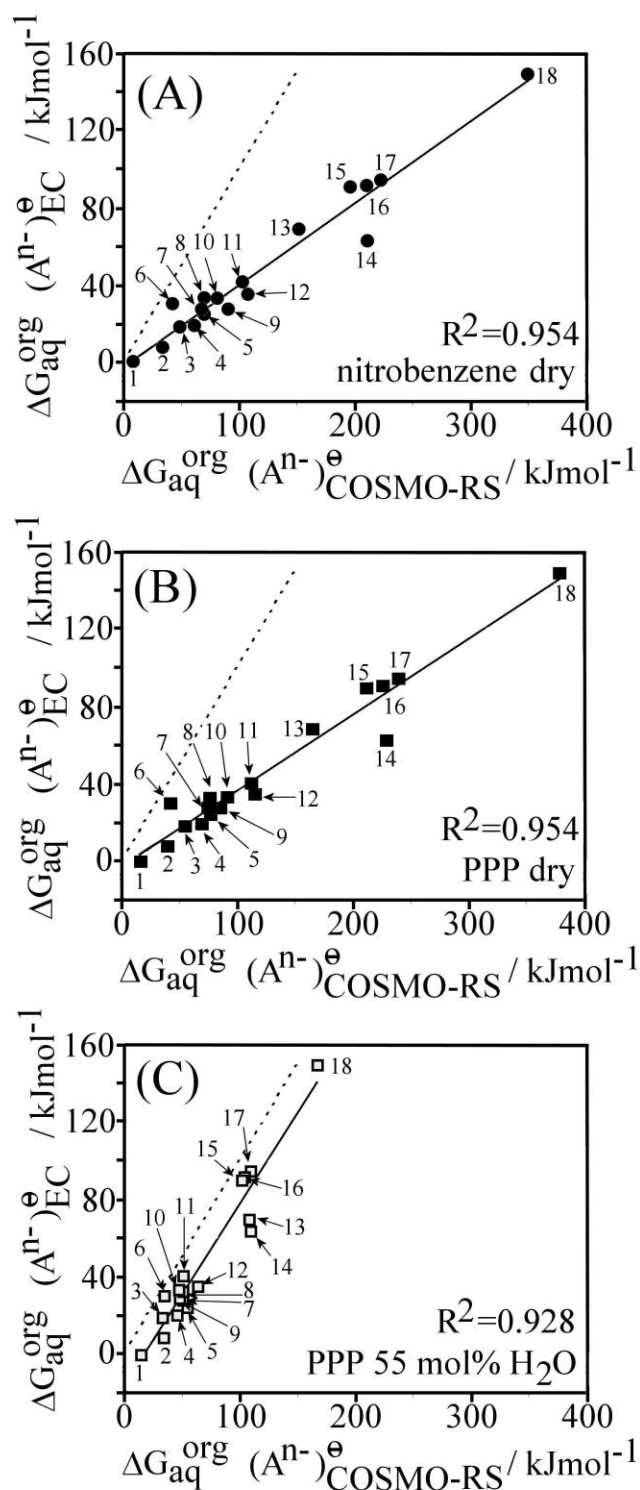
Figure 7. Plots of the calculated transfer Gibbs free energy (based on a COSMOtherm) calculation for (A) the transfer from water to dry nitrobenzene, (B) the transfer from water to dry PPP, and (C) the transfer from water to PPP containing 55 mol% water versus the Gibbs energy for transfer from water to PPP determined by ion transfer voltammetry ($1 = PF_6^-$, $2 = ClO_4^-$, $3 = $ trichloroacetate$^-$, $4 = $ maleateH$^-$, $5 = NO_3^-$, $6 = $ citrateH$_2^-$, $7 = $ malonateH$^-$, $8 = $ succinateH$^-$, $9 = $ fumarateH$^-$, $10 = $ chloroacetate$^-$, $11 = $ acetate$^-$, $12 = Cl^-$, $13 = $ citrateH^{2-}, $14 = $ maleate^{2-}, $15 = $ fumarate^{2-}, $16 = $ succinate^{2-}, $17 = $ malonate^{2-}, $18 = $ citrate^{3-}). The dashed line is the theoretical match and solid lines were fitted.

The calculation of the Gibbs energy of transfer from ion transfer voltammetry data is based on the relationship $\Delta G_{aq}^{\ org}{}_{A^-}^{\ \theta} = nF \, \Delta\phi_{aq}^{\ org}{}_{A^-}^{\ \theta}$ where $\Delta\phi_{aq}^{\ org}{}_{A^-}^{\ \theta} = E_{mid}(1M) - E_{ref}$ and the reference potential E_{ref} is chosen here to bring the transfer potential data into agreement with literature data. In order to visualise the correlation of the resulting data set from electrochemical ion transfer voltammetry results and COSMOtherm calculations plots are constructed (see Figure 7). The plot in Figure 7A shows the correlation of experimental data with COSMOtherm data assuming dry nitrobenzene is the organic phase. Nitrobenzene has been widely used and may be regarded a convenient solvent for comparison with literature data. The correlation is very good but the slope clearly suggests a systematic deviation. The highly charged anions (citrate) show a calculated Gibbs energy of transfer about twice as high as the experimental value. A similarly deviating slope has been reported in the context of pK_a calculations with COSMO-RS [46]. Significant deviations from the trend line are also observed for maleate^{2-} (point 14; this is due to the choice of the data point in the pH7 to pH10 range; the correct value is likely to be close to point 15) and for citrateH$_2^-$ (point 6, this experimental value could only be estimated).

Figure 7B shows a similar plot for the experimental Gibbs energy of transfer data versus COSMOtherm calculations in dry PPP. The similarity of data for dry nitrobenzene and dry PPP is not surprising and linked to the much stronger solvation in the aqueous phase. While the correlation of the experimental results and the COSMO-RS predictions for the transfer from water to PPP is already very satisfying, we wondered about the significantly low slope of the regression line. This led us to the idea to take into account the considerable water content of the organic phase in equilibrium with water, i.e. to use wet PPP instead of dry PPP in the calculations. COSMO-RS predicts the water content to be 40 mol% in wet PPP. Experimental analysis even resulted in 55 mol% water. Taking this water content into account dramatically changes the slope of the correlation line to almost unity, at the cost of slight reduction of the correlation coefficient (see Figure 7C). The loss of correlation

mainly is due to maletae^{2-} (point 14), citrateH$_2^-$ (point 6), and citrateH^{2-} (point 13) but the match with the theoretical line (see dashed line) is now excellent apart from an offset. Overall, the correlation is excellent, and it is especially satisfying that the initial slope inconsistency has been removed by a more realistic description of the experimental situation. i.e. by taking into account the finite water content of the organic phase. Based on this success we expect COSMO-RS prediction of ion transfer energies and potentials for a wider range of solvents, for solvent mixtures, various experimental conditions, and for complex anion structures to be possible in future.

4. Conclusions

It has been shown that liquid | liquid anion transfer of mono-, di-, and tri-carboxylates can be studied experimentally at suitable triple phase boundary electrode systems. Effects of the protonation are clearly linked to the Gibbs free energy of transfer of the more hydrophobic protonated anion species. These are preferentially transferred in some cases even at a pH considerably higher than the corresponding pK$_A$. COSMO-RS calculations offer a powerful predictive tool to provide free energies of transfer or transfer potential information even for more complex molecular anion structures. In future, this tool will be valuable also for visualising the actual transfer process through a solvent composition gradient and for visualising the intermediate transfer stages which could be interface bound.

5. Acknowledgements

6. References

1   A.G. Volkov, D.W. Deamer, *Liquid-liquid interfaces, theory and methods*, CRC Press, New York, 1996.
2   W. Nernst, E.H. Riesenfeld, *Ann. Phys.*, 1902, **8**, 600.
3   H.H.J. Girault, D.J. Schiffrin, *Electroanal. Chem.*, 1989, **15**, 1.

4   Z. Samec, *Pure Appl. Chem.*, 2004, **76**, 2147.

5   J.R. Sandifer (ed.), *Ion-transfer kinetics, Principles and applications*, VCH, Weinheim1995.

6   P. Vanysek, *Electrochemistry at liquid/liquid interfaces,* Springer-Verlag, Berlin, 1985.

7   A. Sherburn, M. Platt, D.W.M. Arrigan, N.M. Boag, R.A.W. Dryfe, *Analyst*, 2003, **128**, 1187.

8   J. Josserand, G. Lagger, H. Jensen, R. Ferrigno, H.H. Girault, *J. Electroanal. Chem.*, 2003, **546**, 1.

9   P. Sun, F.O. Laforge, M.V. Mirkin, *Phys. Chem. Chem. Phys.*, 2007, **9**, 802.

10   P. Sun, F.O. Laforge, M.V. Mirkin, *J. Amer. Chem. Soc.*, 2007, **129**, 12410.

11   R.A.W. Dryfe, *Phys. Chem. Chem. Phys.*, 2006, **8**, 1869.

12   J. Langmaier, Z. Samec, *Electrochem. Commun.*, 2007, **9**, 2633.

13   B. Kralj, R.A.W. Dryfe, *J. Phys. Chem. B*, 2002, **106**, 6732.

14   F. Scholz, U. Schröder, R. Gulaboski, *Electrochemistry of immobilized particles and droplets*, Springer, Berlin, 2005.

15   F. Marken, R.D. Webster, S.D. Bull, S.G. Davies, *J. Electroanal. Chem.*, 1997, **437**, 209.

16   R. Gulaboski, V. Mirceski, F. Scholz, *Electrochem. Commun.*, 2002, **4**, 277.

17   F. Quentel, C. Elleouet, V. Mirceski, V.A. Hernandez, M. L'Her, M. Lovric, S. Komorsky-Lovric, F. Scholz, *J. Electroanal. Chem.*, 2007, **611**, 192.

18   M.J. Bonné, C. Reynolds, S. Yates, G. Shul, J. Niedziolka, M. Opallo, F. Marken, *New J. Chem.*, 2006, **30**, 327.

19   A.O. Simm, F.G. Chevallier, O. Ordeig, F.J. del Campo, F.X. Munoz, R.G. Compton, *ChemPhysChem*, 2006, **7**, 2585.

20   T.J. Davies, A.C. Garner, S.G. Davies, R.G. Compton, *ChemPhysChem*, 2005, **6**, 2633.

21   D. Rayner, N. Fietkau, I. Streeter, F. Marken, B.R. Buckley, P.C.B. Page, J. del Campo, R. Mas, F.X. Munoz, R.G. Compton, *J. Phys. Chem. C*, 2007, **111**, 9992.

22   E. Bak, M. Donten, Z. Stojek, F. Scholz, *Electrochem. Commun.*, 2007, **9**, 386.

23   M.A. Ghanem, F. Marken, *Electrochem. Commun.*, 2005, **7**, 1333.

24   J. Niedziolka, K. Szot, F. Marken, M. Opallo, *Electroanalysis*, 2007, **19**, 155.

25   S.M. MacDonald, J.D. Watkins, Y. Gu, K. Yunus, A.C. Fisher, G. Shul, M. Opallo, F. Marken, *Electrochem. Commun.*, 2007, **9**, 2105.

26   S.M. MacDonald, P.D.I. Fletcher, Z.G. Cui, M. Opallo, J.Y. Chen, F. Marken, *Electrochim. Acta*, 2007, **53**, 1175.

27   F. Marken, K.J. McKenzie, G. Shul, M. Opallo, *Faraday Disc.*, 2005, **129**, 219.

28   R. Gulaboski, F. Scholz, *J. Phys. Chem. B*, 2003, **107**, 5650.

29   R. Gulaboski, V. Mirceski, F. Scholz, *Amino Acids*, 2003, **24**, 149.

30   F. Scholz, *Annu. Rep. Prog., Sec. C*, 2006, **102**, 43.

31   S. Komorsky-Lovric, K. Riedl, R. Gulaboski, V. Mirceski, F. Scholz, *Langmuir*, 2002, **18**, 8000.

32   U. Schröder, J. Wadhawan, R.G. Evans, R.G. Compton, B. Wood, D.J. Walton, R.R. France, F. Marken, P.C.B. Page, C.M. Hayman, *J. Phys. Chem. B*, 2002, **106**, 8697.

33   N. Katif, S.M. MacDonald, A.M. Kelly, E. Galbraith, T.D. James, A.T. Lubben, M. Opallo, F. Marken, *Electroanalysis*, 2008, in print.

34   A. Klamt, *J. Phys. Chem.,* 1995, **99**, 2224.

35 A. Klamt, V. Jonas, T. Buerger, J.C.W. Lohrenz, *J. Phys. Chem. A,* 1998, **102**, 5074.

36 A. Klamt, COSMO-RS from quantum chemistry to fluid phase thermodynamics and drug design, Elsevier: Amsterdam, 2005.

37 A. Klamt, G.J. Schüürmann, *J. Chem. Soc., Perkin Trans. 2*, 1993, 799.

38 R. Ahlrichs, M. Bär, H.P. Baron, R. Bauernschmitt, S. Böcker, M. Ehrig, K. Eichkorn, S. Elliott, F. Furche, F. Haase, M. Häser, H. Horn, C. Hattig, C. Huber, U. Huniar, M. Kattannek, M. Köhn, C. Kölmel, M. Kollwitz, K. May, C. Ochsenfeld, H. Öhm, A. Schäfer, U. Schneider, O. Treutler, M. von Arnim, F. Weigend, P. Weis, H. Weiss, Turbomole Version 5.6 (2002).

39 A.D. Becke, *Phys. Rev. A*, 1988, **38**, 3098.

40 J.P. Perdew, *Phys. Rev. B,* 1986, **33**, 8822.

41 F. Eckert, A. Klamt, COSMO*therm*, Version C2.1-Revision 01.07; COSMO*logic* GmbH&CoKG, Leverkusen, Germany (2007).

42 F. Scholz, U. Schröder, R. Gulaboski, *Electrochemistry of immobilized particles and droplets*, Springer, Berlin, 2005, p. 213.

43 Y. Marcus, *Ion properties*, Marcel Dekker, New York, 1997.

44 F. Marken, C.M. Hayman, P.C.B. Page, *Electrochem. Commun.*, 2002, **4**, 462.

45 D.R. Lide, *Handbook of chemistry and physics*, 74th ed., 1993-1994, CRC Press, London, 1992, 8-45.

46 A. Klamt, F. Eckert, M. Diedenhofen, M.E. Beck, *J. Phys. Chem. A.*, 2003, **107**, 9380.